# ANNUAL REPORT
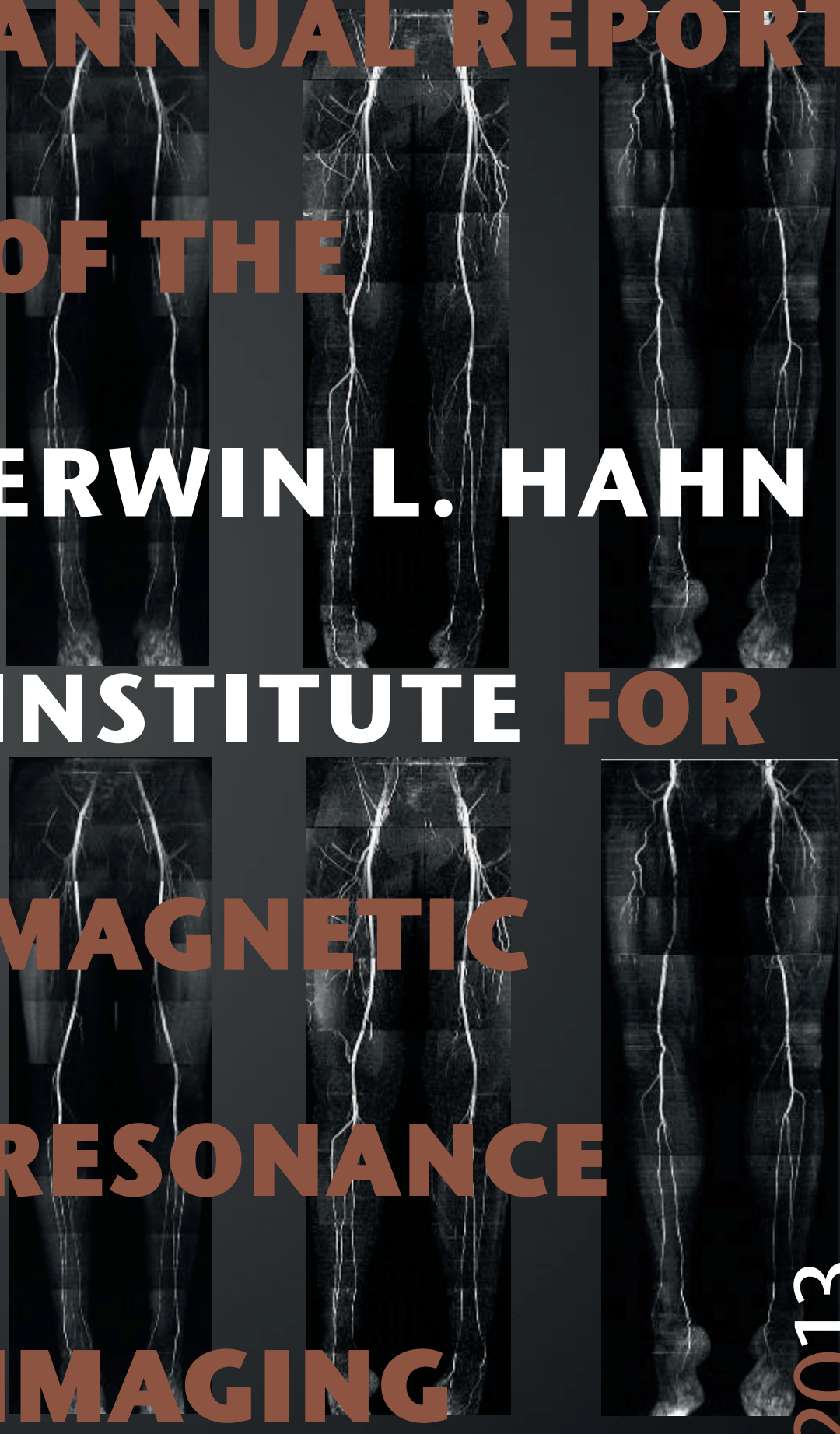
## OF THE

# ERWIN L. HAHN

# INSTITUTE FOR

## MAGNETIC

## RESONANCE

## IMAGING

2013

# Preface

This year has seen a number of important changes at the Erwin L. Hahn Institute. The first of which was the decision of Mark Ladd to accept a new challenge as head of the department of Medical Physics in Radiology at the German Cancer Research Institute in Heidelberg. We are of course very sad to see Mark leave Essen, and wish him every success in his new position. Mark has not entirely left us, as his ERC Advanced Grant will still be conducted in Essen, and he will remain a Principal Investigator at the Erwin L. Hahn Institute for the duration of the project. The second major news item is that Mark's position as director will be taken by Harald Quick who has decided to return to Essen to accept a new chair in the Medical Faculty. He will commence work at the Institute in February 2014.

This year saw another successful Erwin L. Hahn lecture on functional MRI, given by Kamil U␣urbil of the Center or Magnetic Resonance Research in Minnesota. This was the centre-piece of a one day workshop on fMRI, and was followed by an ESMRMB course on multiband imaging. After the lecture Mark Ladd received the Erwin L. Hahn Award for his enormous contributions to the Institute over many years.

Despite the many changes the research of the Institute continued to flourish with impressive new results to be seen in this report. The research of the Institute led to ?? publications. The staff of the Institute now counts 18 who are permanent in the Institute, and we shall be restructuring the Institute in 2014 in order to accommodate them.

I hope you enjoy reading this short report of our progress and activities in 2013.

*David Norris*

Essen, January 2014
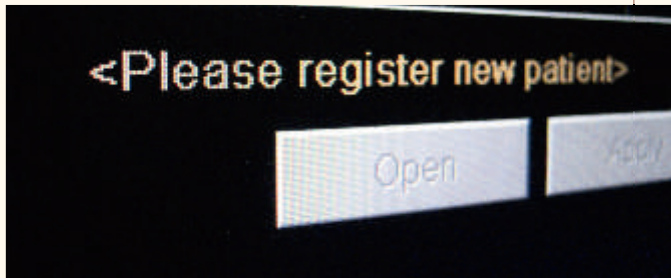
## Erwin L. Hahn Institute for Magnetic Resonance Imaging

Arendahls Wiese 199
D-45141 Essen
Germany

t ++49 (0)201-183-6070
f ++49 (0)201-183-6073
w www.hahn-institute.de

# Peripheral vascular imaging

*Anja Fischer*

## Non-contrast-enhanced MRA of the lower extremity arteries at 7 Tesla

For evaluation of the arteries of the lower extremity, digital subtraction angiography (DSA) with the intra-arterial injection of iodinated contrast media is the established gold standard. Over the last 20 years, MR angiography (MRA) with venous administration of gadolinium (Gd)-based contrast media has evolved to become an excellent alternative diagnostic tool for the assessment of vessel pathologies. In clinical routine, the standard magnetic field strength for angiography of the lower extremity still lies at 1.5 T. The recognition of Nephrogenic Systemic Fibrosis (NSF) a few years ago has implicated that alternatives for the evaluation of patients with renal failure have been sought, as gadolinium plays a triggering role for the development of NSF[1]. Owing to this development, attention has recently focused on new, non-enhanced MR angiographic techniques for the assessment of the lower extremity vessels without the need of any contrast media. Several non-enhanced MR angiography techniques have been discussed, mostly based on turbo spin echo or steady-state free precession imaging [2,3]. Owing to the ongoing development of multi-channel body radiofrequency (RF) coils and shimming technology at 7 T, the initial interest in brain and musculoskeletal imaging has expanded to whole-body applications, and the aim of our research was to investigate the feasibility of non-enhanced 7 T MRA of the lower extremities.

In a first feasibility study, eight healthy volunteers were examined (4 female, 4 male subjects). The average age was 27.0 years with a range of 21 to 35 years. Ultra-high-field examinations were performed on the 7 T whole-body MR system of our institute (Magnetom 7T, Siemens Healthcare, Erlangen, Germany). All volunteers were examined in feet-first supine position on a custom-built AngioSURF table [4,5], which was manually positioned between the stationary RF coil system for multi-station imaging (Fig. 1). A custom-built 16-channel transmit / receive coil was utilized, consisting of 16 microstrip elements with meanders [6]. Five elements were positioned flat under the AngioSURF table; the other 11 elements were arranged in a semicircle above the table. The coil was driven by an 8-channel RF shimming system [7] using a 16-channel planar butler matrix and a variable power combiner (VPC) to obtain splitting of one high-frequency signal into 16 individual channels. For the first MR imaging of the lower extremity arteries at 7 T, a two-dimensional (2D) non-enhanced T1-weighted spoiled gradient echo sequence (FLASH) was acquired with and without a venous saturation pulse. Time-Interleaved Acquisition of Modes (TIAMO) [8] was integrated to reduce B1 artifacts and to obtain near homogeneous image quality of the arteries. Visual qualitative image analysis was carried out with regard to overall image quality of the arterial segments. The presence of artifacts and impairment due to venous overlay were assessed as well. Contrast ratios were obtained for each artery segment for quantitative evaluation.

Both T1-weighted spoiled gradient echo sequences without and with venous saturation pulses provided a largely homogeneous, hyperintense delineation of the arteries in the iliac, femoral, popliteal, and lower leg segments without application of contrast agent (Fig. 2). The large arteries of the pelvis and lower extremity as well as small pedal and intramuscular vessels could be delineated in overall moderate to good image quality. The best image quality scores were achieved for the external iliac and the popliteal segments. 2D FLASH imaging with venous saturation pulses enabled an adequate saturation of surrounding muscle and fat; it also showed strong superiority with regard to the presence of venous overlay.
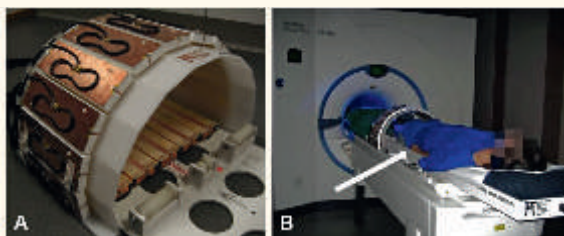


*Fig. 1: 7 T MRA examinations were performed with a custom-built 16-channel transmit / receive coil (A). The coil consists of 16 meander elements, with five elements placed dorsally on the base of the integrated scanner table in a sliding frame, whereas eleven elements were arranged semicircularly above (A). For imaging of the lower extremity arteries, a manually positionable AngioSURF table (arrow) was slid between the two coil sections. In this way, multi-station imaging was possible to capture the entire vasculature from pelvis to feet (B).*

These initial results demonstrate the feasibility of non-enhanced MR angiography of the lower extremity arteries at the ultra-high field strength of 7 T in healthy subjects. To our knowledge, this is the first feasibility study with 7 T MRI covering such a large extent of the body in one examination. On the other hand, our first experiences with non-contrast-enhanced arterial imaging at 7 T revealed limitations and challenges of this emerging imaging technique as well. One issue is a consistent signal loss in the middle third of the thigh, which is suspected to be caused by RF interferences inside the 16-channel coil due to the variable anatomy of pelvis and legs along the longitudinal axis. This problem might be addressed by utilizing dedicated TIAMO shims [9] in these imaging stations. A second issue is periodic vessel signal declines over short segments that can be best appreciated in the coronal MIP images; these signal declines were a major problem for 2D FLASH imaging, as this sequence was not cardiovascular gated.

The mentioned challenges were addressed with further sequence optimization, resulting in a modified phonocardiogram-gated Turbo-FLASH sequence with additional application of individual TIAMO shims. A follow-up volunteer study was conducted and this sequence showed superiority regarding image quality and artery contrast [10] (Fig. 3). In a current study, non-contrast-enhanced Turbo-FLASH imaging at 7 T is being performed in patients with known peripheral arterial occlusive disease (PAOD), as there is a high prevalence of chronic renal impairment and the necessity of dialysis in patients with PAOD due to the association of PAOD with diabetes. Images are being compared to contrast-agent-based MRA at 1.5 T and the presence of arterial stenosis and occlusions counted for each artery segment in both MRA techniques. Initial results in a small patient group demonstrate acceptable performance of non-enhanced 7 T MRA [11].

The future of 7 T non-enhanced T1-weighted MRA might lie in specific applications in the lower extremity vessels, which will be addressed in current and upcoming trials at the Erwin L. Hahn Institute.

For further details please see Fischer A, Maderwald S, Orzada S, Johst S, Schäfer LC, Ladd ME, Nassenstein K, Umutlu L, Lauenstein TC. Nonenhanced magnetic resonance angiography of the lower extremity vessels at 7 tesla: initial experience. Invest Radiol. 2013. 48(7):525-34.
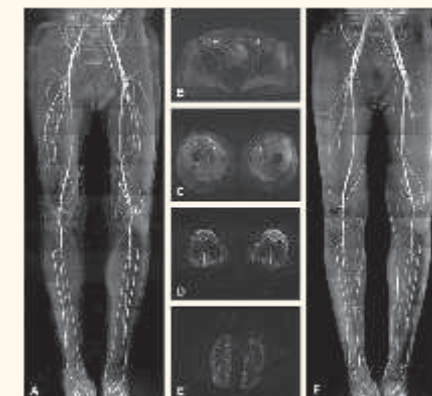


*Fig. 2: T1-weighted 2D FLASH imaging with venous saturation pulses enabled a largely homogeneous, hyperintense delineation of the arteries with saturation of surrounding tissue and veins in all analyzed vessel segments. Figure A shows a coronal MIP of the entire examined territory (male, 1.85 m, 85 kg). Figure B to D are the axially acquired source images of the iliacal, femoral, and popliteal segments. Even the small arteries of the ankle are depicted (E). A data set without venous saturation (F) in the same subject yielded strong venous overlay in the iliac and femoral region.*
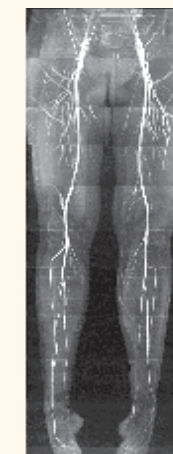


*Fig. 3: 7 T non-enhanced MR angiography of the lower extremity arteries in a healthy volunteer, again utilizing the manually positionable AngioSURF table and the 16-channel transmit/receive body coil. Cardiac gating was additionally performed utilizing a phonocardiogram to enable a more homogeneous hyperintense artery signal from pelvis to feet. Acquisition of an entire angiogram amounted to 20-30 min.*

# Proton Spectroscopy of the brain at 7T

*Tom Scheenen*

## Multi-center reproducibility of neurochemical profiles in the human brain at 7 Tesla

With proton magnetic resonance spectroscopy ($^1$H-MRS) cerebral metabolite and neurotransmitter concentrations can be measured *in vivo*. This tool has been used for many years, and is currently increasingly being utilized in basic neuroscience research, next to existing clinical applications. While improvements in precision of metabolite quantification at ultra-high fields were reported in individual laboratories, the between-site and vendor reproducibility of neurochemical profiling, critical for widespread utility of the methodology, has not been assessed. Initiated from Essen, we determined the reproducibility of current state-of-the-art single voxel $^1$H-MRS in healthy volunteers in a multi-center setting at 7 Tesla.

Seven healthy subjects were each examined twice on four 7T whole body systems in Europe and in the USA. The institutions and scanner configurations were:

1) Erwin L. Hahn Institute (ELH), University Duisberg-Essen, Essen, Germany; Siemens
2) Center for Magnetic Resonance Research (CMRR), University of Minnesota, Minneapolis, Minnesota, USA; Siemens
3) C.J. Gorter Center for High Field MRI, Department of Radiology, University Medical Center Leiden (LUMC), Leiden, the Netherlands; Philips
4) Department of Radiology, University Medical Center Utrecht (UMCU), Utrecht, the Netherlands; Philips

All systems were equipped with exactly the same short-echo time semi-LASER pulse sequence and the same sequence parameters. Voxel repositioning in the same subjects was done manually. Neurochemical profiles were obtained from the posterior cingulate cortex (GM) and the corona radiata (WM) and were analyzed with LCModel. After quality control of the spectra, a variance component analysis was used to determine sources of variation in the metabolite concentrations. Calculated metabolite concentrations from the neurochemical profiles were in line with existing literature. Concentrations of 12 out of 16 reliably quantified metabolites were compared between institutes and variation in the data was assigned to different contributing factors. Concentration variations in Glutamate (Glu, GM only), myo-Inositol (mI), scyllo-Inositol (sI, GM only) total Creatine (tCr, WM only) & total Choline (tCho) were addressed to inter-subject differences. Variations in N-Acetyl aspartate + N-Acetyl aspartate glutamate (tNAA), Glutathione (GSH), Glutamine (Gln) and Glu (WM only) occurred because of institutional differences (different MR systems). The remaining metabolites had various sources of variance, including systematic noise. Repeated measures showed reproducible results, except for Alanine (Ala), Glu, GSH and sI (white matter only, test-retest significant difference $P<0.05$), and Ascorbate/vitamin C (Asc, gray matter, $P<0.001$ & white matter, $P<0.01$). Test-retest coefficients of variation remained below 5% for tNAA, tCr, tCho, mI and Glu and below 25% for Asc, Aspartate, GABA, Gln, GSH, Glycine (GM only), Phosphorylethanolamine, sI and Glucose + Taurine, except for Ala (<31%) and Lactate (<36%).

We established the within- and between-subject and between-institution reproducibilities in measurements of *in-vivo* neurochemical profiles at 7T, which may be used as a guidance for the (im)possibilities of quantifying metabolite and neurotransmitter concentrations with 1H-MRS at 7 Tesla. Furthermore, we showed that an institute independent reproducible detection was possible, and that variations between subjects and institutions could be detected accurately.
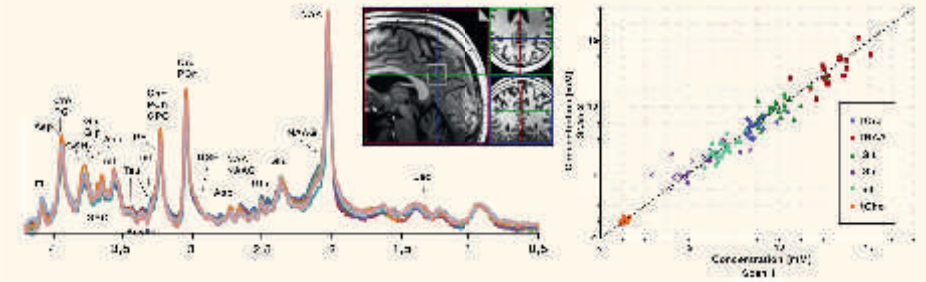


*Fig.4: MR spectra of the gray matter of all seven volunteers at one MR system. All peaks are assigned to the corresponding metabolites, and the spectra are normalized to the NAA amplitude. The image insert shows the position of the voxel. The graph illustrates the test-retest reproducibility of the largest metabolites in gray matter of all volunteers.*

| LCModel results | Metabolite: | Asc | Asp | GABA | Gln | Glu | GSH | mI | Lac | PE | Scyllo | NAA+NAAG | Cre+PCr | Glc+Tau | GPC+PCh |
|---|---|---|---|---|---|---|---|---|---|---|---|---|---|---|---|
| **Posterior Cingulate Cortex (primarily gray matter)** | Mean (mM) | 2.0 | 3.8 | 1.3 | 5.2 | 9.3 | 1.2 | 6.4 | 0.8 | 1.6 | 0.3 | 12.0 | 8.1 | 2.2 | 1.3 |
| | SD (mM) | 0.3 | 0.6 | 0.4 | 1.1 | 0.8 | 0.3 | 0.6 | 0.3 | 0.3 | 0.1 | 1.0 | 0.5 | 0.6 | 0.1 |
| | CoV (%) | 8.8 | 8.8 | 22.2 | 8.3 | 2.9 | 14.5 | 4.0 | 35.2 | 12.9 | 12.7 | 3.1 | 2.9 | 14.0 | 4.2 |
| | mean CRLB (%SD) | 14.2 | 14.3 | 28.6 | 6.4 | 3.1 | 13.2 | 4.1 | 23.8 | 11.8 | 20.2 | 1.3 | 1.9 | 13.4 | 4.2 |
| | N (after QC) | 53 | 53 | 32 | 53 | 53 | 53 | 53 | 32 | 53 | 52 | 53 | 53 | 47 | 53 |
| **Corona Radiata (primarily white matter)** | Mean (mM) | 1.9 | 2.8 | 1.3 | 2.4 | 7.0 | 1.2 | 6.0 | 0.9 | 1.3 | 0.3 | 13.3 | 7.6 | 1.2 | 1.9 |
| | SD (mM) | 0.5 | 0.6 | 0.4 | 0.9 | 0.9 | 0.3 | 0.8 | 0.3 | 0.3 | 0.1 | 1.2 | 0.4 | 0.6 | 0.3 |
| | CoV (%) | 16.2 | 15.9 | 17.7 | 17.7 | 3.4 | 11.5 | 4.2 | 31.5 | 14.8 | 20.8 | 2.1 | 2.7 | 22.8 | 3.4 |
| | mean CRLB (%SD) | 15.0 | 20.3 | 30.9 | 15.5 | 3.9 | 12.6 | 3.6 | 22.3 | 13.5 | 20.7 | 1.2 | 2.0 | 19.2 | 3.3 |
| | N (after QC) | 54 | 53 | 35 | 44 | 48 | 54 | 54 | 48 | 54 | 44 | 54 | 54 | 53 | 54 |

*Tab. 1: Mean concentrations and standard deviations (SD) in mM of all quantifiable metabolites detected with reasonable precision of the fit (Cramér-Rao Lower bound < 50% (CRLB)). Also listed are the mean coefficient of variations (CoV), the mean CRLB and the number of spectra (N) out of in total 53 GM and 54 WM spectra (5 exclusions) that contributed to each mean after quality control. Concentrations, CoVs and CRLBs are only reported when at least 25% of the datasets for each ROI passed quality control. All reported values are corrected for T2, magnetization transfer effects and partial volume.*

# Reduced power deposition in RARE/TSE imaging of the human head

## A new approach for T2-weighted imaging at 7 Tesla

*David G. Norris*
*Rasim Boyacıoğlu*
*Jenni Schulz*
*Markus Barth*
*Peter J. Koopmans*

The RARE/TSE imaging sequence (1), is one of the most important methods for clinical imaging, because of its speed, high image quality, sensitivity and T2-contrast (2). The high image quality is to a large extent attributable to the fact that spin-echoes are exclusively used to generate the signal, hence to a very large degree eliminating the deleterious effects of inhomogeneities in the static magnetic field. An unfortunate corollary of the use of spin echoes is the large number of refocusing pulses required, which result in a high RF power deposition. Given the roughly quadratic dependency of power deposition on field strength (3) this leads to the paradoxical situation that at the field strengths where spin-echo sequences offer potentially the greatest benefit in terms of improved image quality their application is most limited by power deposition considerations.

In this project we explored the power reduction possible if multiband imaging, also known as simultaneous multi-slice imaging (4), is used to excite and refocus multiple slices simultaneously. The traditional method of generating RF pulses for multiband imaging requires the superposition of N pulses in the time domain, with each pulse having a unique phase-gradient corresponding to the position of the corresponding slice (5,6). This approach means that the power deposition of the multiband pulse is proportional to N. We recently introduced a family of RF-pulses that go under the acronym PINS (power independent of number of slices, (7)) that rely on periodic excitation to circumvent the increased power deposition of the traditional approach. The periodic nature of the PINS pulses means that the number of slices excited is only limited by the dimensions of the radio-frequency coils used. The higher the number of slices, the greater will be the power reduction achievable, and the better the slice profile (7). Hence, we also applied the blipped CAIPIRINHA method (often abbreviated to blipped CAIPI) to RARE/TSE, in order to potentially reduce the gap between adjacent slices and improve the quality of the multiband image reconstruction (8).

Experimental work was conducted at the Erwin L Hahn Institute on healthy volunteers using a 32 channel send receive coil (Nova medical, Wilmington, USA). A standard RARE/TSE sequence was modified to replace the manufacturer's RF pulses with PINS pulses for both excitation and refocusing as shown in Fig. 5. Optionally additional gradient pulses for the application of blipped CAIPI were included, shown schematically as shaded gradient pulses in Fig. 5. Data were acquired in sagittal section as transaxial slices would excite an undefined number of slices beyond the extent of the RF-receiver coils, which in the past have proven impossible to reconstruct. In preliminary experiments we found that it is possible to use a rapid FLASH acquisition to obtain the reference data necessary to reconstruct the multiband data.
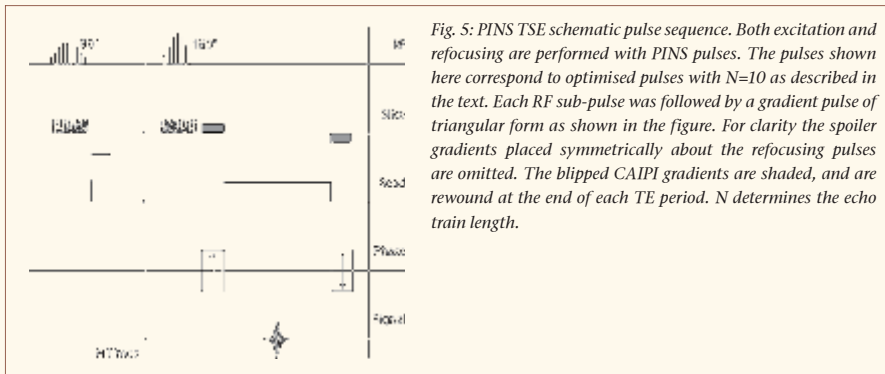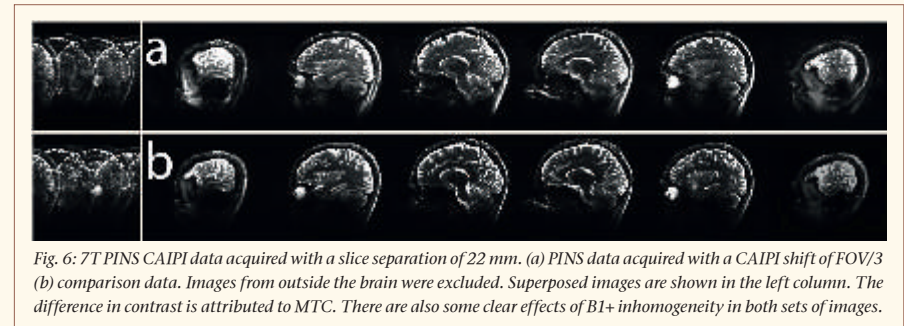


*Fig. 5: PINS TSE schematic pulse sequence. Both excitation and refocusing are performed with PINS pulses. The pulses shown here correspond to optimised pulses with N=10 as described in the text. Each RF sub-pulse was followed by a gradient pulse of triangular form as shown in the figure. For clarity the spoiler gradients placed symmetrically about the refocusing pulses are omitted. The blipped CAIPI gradients are shaded, and are rewound at the end of each TE period. N determines the echo train length.*

At 7T the session commenced with a set of reference images, after which standard shim and B1-calibration procedures were performed. 3D-FLASH reference data were acquired at the start and at the end of the session. TSE comparison images were acquired with a TR/TE/TA of 15910 ms/52 ms/509 s, with a field of view of 250mm and an acquisition matrix of 256 by 256, using 120° refocusing pulses with the SAR monitor on 100%. The PINS data were acquired using TR/TE/TA of 8000 ms/46 ms/128 s and an ETL of 16, blipped CAIPI (FOV/3), a slice period of 22mm, and otherwise identical geometric parameters to the comparison data. The SAR monitor level was 80% for this protocol.

All PINS data were reconstructed offline in MATLAB. Superposed slices were unaliased with an in-house implementation of the SLICE-GRAPPA algorithm using a 4x3 kernel (8). The image quality of the PINS and the comparison data is similar as is shown in Fig. 6. The higher contrast in the comparison data is caused by the fact that



*Fig. 6: 7T PINS CAIPI data acquired with a slice separation of 22 mm. (a) PINS data acquired with a CAIPI shift of FOV/3 (b) comparison data. Images from outside the brain were excluded. Superposed images are shown in the left column. The difference in contrast is attributed to MTC. There are also some clear effects of B1+ inhomogeneity in both sets of images.*

there is no MTC effect when PINS pulses are used.

It was thus possible to demonstrate a considerable reduction in RF power deposition for RARE/TSE sequences through the use of PINS pulses, combined with blipped CAIPI. It is to be expected that this technique will largely eliminate the SAR restrictions currently experienced by standard RARE/TSE sequences at ultra high static magnetic field strengths. The PINS method can also be applied to any original RF-pulse form, including adiabatic pulses, and is thus capable of generating a broad range of contrasts. It will hence be possible to perform inversion recovery TSE experiments within acceptable acquisition times, including STIR-TSE (9).

Hitherto multiband imaging has been seen as a means of significantly accelerating the acquisition of EPI data, and PINS pulses primarily viewed as a means of ameliorating the high SAR and peak RF voltages associated with traditional multiband pulses. The current paper demonstrates that multiband imaging combined with PINS pulses can be used to achieve a substantial reduction in SAR, which should lead to considerable improvements in scanner performance at 7T.

References
1.  Hennig J, Nauerth A, Friedburg H. RARE imaging: A fast imaging method for clinical MR. Magn Reson Med 1986;3:823-833.
2.  Mulkern RV, Wong STS, Winalski C, Jolesz FA. Contrast Manipulation and Artifact Assessment of 2D and 3D RARE Sequences. Magn Reson Imag 1990;8:557-566.
3.  Vaughan JT, Garwood M, Collins CM, Liu W, De la Barre L, Adriany G, Andersen P, Merkle H, Goebel R, Smith MB, Ugurbil K. 7T vs. 4T: RF power, homogeneity, and signal-to-noise comparison in head images. Magn Reson Med 2001;46(1):24-30.
4.  Larkman DJ, Hajnal JV, Herlihy AH, Coutts GA, Young IR, Ehnholm G. Use of multicoil arrays for separation of signal from multiple slices simultaneously excited. J Magn Reson Imag 2001;13(2):313-317.
5.  Müller S. Multifrequency Selective RF Pulses for Multislice MR Imaging. Magn Reson Med 1988;6:364-371.
6.  Maudsley AA. Multiple-line-scanning spin-density imaging. Journal of Magnetic Resonance 1980;41(1):112-126.
7.  Norris DG, Koopmans PJ, Boyacioglu R, Barth M. Power Independent of Number of Slices (PINS) Radiofrequency Pulses for Low-Power Simultaneous Multislice Excitation. Magn Reson Med 2011;66(5):1234-1240.
8.  Setsompop K, Gagoski BA, Polimeni JR, Witzel T, Wedeen VJ, Wald LL. Blipped-controlled aliasing in parallel imaging for simultaneous multislice echo planar imaging with reduced g-factor penalty. Magn Reson Med 2012;67(5):1210-1224.
9.  Constable RT, Smith RC, Gore JC. Signal-to-noise and contrast in fast spin-echo (FSE) and inversion recovery FSE imaging. J Comp Assist Tomogr 1992;16(1):41-47.

# Functional Brain Imaging

Bettina Gathmann

Does stress always impair our decision-making performance?
Neural correlates of the interaction of stress, executive functions, and decision making under risk

A key function in human's everyday life is decision making. Most of the time we do not think a lot about the decisions we make, for example to take a zip of tea out of our tea cup next to us. Those decisions are without far-reaching consequences, and easy to make. However, in some situations people have to make decisions with potentially severe consequences, for example, a doctor in the operating room or a policeman during a street fight. These situations often elicit psychological stress, which could have an influence on the decisions people make. Additionally, these situations often require simultaneous actions while making a crucial decision. It is important to understand what happens to peoples' decision-making performance in such situations. So far, research has shown that stress as well as additional load on the executive system, produced by a parallel working memory task, impair decision making under risk [1-3]. However, the combination of stress and additional load seems to preserve the decision-making performance from decreasing, probably by a switch from serial to parallel processing [4]. The question remains what happens in the brain in such demanding situations and which brain areas are involved in decision making under stress in a dual-task situation?

We hypothesized that stress would lead to changes of neural activity in brain areas involved in making decisions under risk and working memory, i.e. dorsolateral prefrontal areas and parts of the anterior cingulate cortex [5, 6]. Additionally, these regions are known to be involved in the executive control mechanisms [7, 8], which in turn are presumed to be engaged in the serial-to-parallel shift. Therefore, we assumed an association between the serial-to-parallel shift and areas of the dorsolateral prefrontal cortex (dlPFC) as well as the anterior cingulate cortex (ACC). We analyzed data from 33 right-handed, healthy participants, randomly assigned to the stress group (n = 16) and the control group (n = 17). The groups did neither differ significantly regarding gender nor age. We used the ELH's 7-tesla whole-body MRI system (Magnetom 7T, Siemens Healthcare, Erlangen, Germany) in order to investigate the underlying neural correlates of the interaction of stress (induced by the Trier Social Stress Test [9]), risky decision making (Game of Dice Task, GDT; [10]), and a parallel executive task (2-back task, similar to the one used by [11]) to get a better understanding of the above mentioned behavioral findings. For this experiment, the scanner was equipped with a 32-channel transmit/receive head coil (Nova Medical, Wilmington, USA). Whole functional MRI images

were acquired with an optimized bold contrast-sensitive EPI sequence [c.f. 12]. Based on prior hypotheses, we conducted region of interest (ROI) analyses in the prefrontal cortex, in particular in the dlPFC (Brodmann areas 9, 10, and 46), the ACC (Brodmann areas 24 and 32), and the parietal cortex (Brodmann areas 5 and 7). General linear models (GLMs) were applied to the time course of activation, where stimulus onsets were modeled as single-impulse response functions. Linear contrasts of parameter estimates were defined to test specific effects.

The results show that on a behavioral level, stressed participants did not show significant differences in task performance [c.f. 4]. Interestingly, when comparing the stress group with the control group, the stress group showed a greater increase in neural activation in BA 10 - the more anterior part of the dorsolateral prefrontal cortex (dlPFC) - when performing the 2-back task simultaneously with the GDT than when performing each task alone (see Fig. 7). This brain area is associated with parallel processing [13]. Additionally, we found that in the stress group the increase of cortisol concentration is negatively correlated with the increase of activation in the BA 9 (the more dorsal part of the dlPFC) regarding the contrast GDT plus 2-back > GDT (see Fig. 8). This indicates that in the stress group an increase of stress level is associated with a decrease of neural activation in the dorsal part of the dlPFC during the GDT plus 2-back task compared with the GDT. This brain region was found to be associated with serial processing of information [14]. The combination of those findings may point in the following direction: In stressful dual-tasking situations, where a decision has to be made when in parallel working memory is demanded, a stronger activation of a brain area associated with parallel processing (anterior part of the dlPFC) takes place. Simultaneously, brain areas associated with serial processing (dorsal part of the dlPFC) are related to a decrease of activation. The findings are in line with the idea that stress seems to trigger a switch from serial to parallel processing in demanding dual-tasking situations [c.f. 4, 15].

This project was done in cooperation between the Department of Cognitive Psychology, Ruhr-University Bochum (Prof. Oliver T. Wolf) and the Department of General Psychology: Cognition, University of Duisburg-Essen (Prof. Dr. Matthias Brand). This project was funded by the German Research Foundation (BR 2894/6-1 and WO773/11-1).
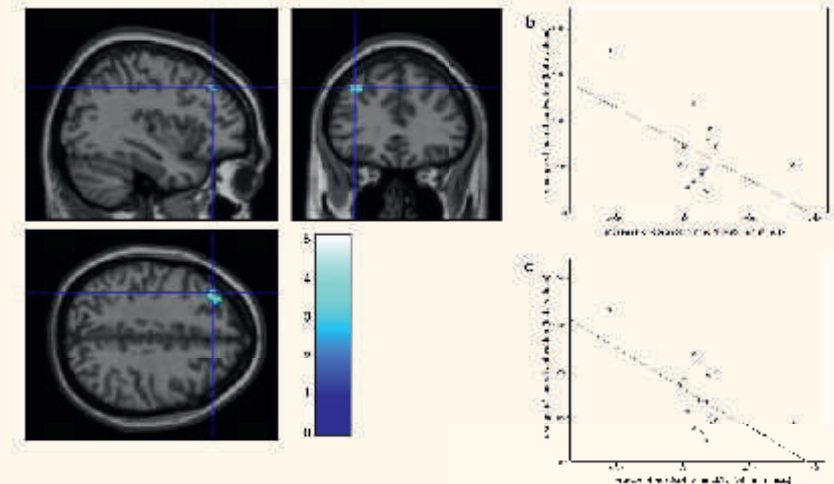


Fig. 8: a) Increasing cortisol concentration in the stress group is related with a deactivation in the dorsal part of the dlPFC (BA 9) during the GDT plus 2-back when compared with the GDT. The fixing cross was set at MNI-coordinate 1(x = -36, y = 34, z = 42). The plot of the negative correlation between increase of cortisol in the stress group (from baseline to time point +95 min) and brain activation b) at the MNI-coordinate 1 and c) at the MNI coordinate 2 ( x = -30, y = 43, z = 40)
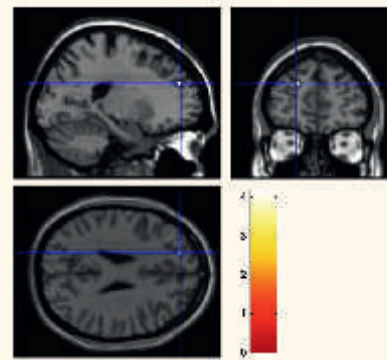


Fig. 7: Results of the dual-task effect (GDT plus 2-back > GDT) in the stress group compared to the control group at a threshold of p≤ .001 (uncorrected) and an applied extended threshold of k ≥ 10 voxel: Activation in the anterior part of the dlPFC (BA 10).

References
1. Starcke, K., et al., Cognitive Processing, 2011. 12: p. 177–182.
2. Starcke, K., et al., Behavioral Neuroscience, 2008. 122: p. 1352–1360.
3. Starcke, K. and M. Brand, Neuroscience & Biobehavioral Reviews, 2012. 36: p. 1228–1248.
4. Pabst, S., et al., Behavioral Neuroscience, 2013: p. 369–379.
5. Labudda, K., et al., Experimental Brain Research, 2008. 187: p. 641–650.
6. Owen, A.M., et al., Human Brain Mapping, 2005. 25: p. 46–59.
7. Alvarez, J.A. and E. Emory, Neuropsychology Review, 2006. 16: p. 17–42.
8. D'Esposito, M., et al., Nature, 1995. 378: p. 279–281.
9. Kirschbaum, C., K.M. Pirke, and D.H. Hellhammer, Neurospsychobiology, 1993. 28: p. 77–81.
10. Brand, M., et al., Neuropsychology, 2005. 19: p. 267–277.
11. Schoofs, D., D. Preuß, and O.T. Wolf, Psychoneuroendocrinology, 2008. 33: p. 643–653.
12. Poser, B.A., et al., NeuroImage, 2010. 51: p. 261–266.
13. Koechlin, E. and A. Hyafil, Science, 2007. 318: p. 594–598.
14. Dux, P.E., et al., Neuron, 2006. 52: p. 1109–1120.
15. Plessow, F., A. Kiesel, and C. Kirschbaum, Experimental Brain Research, 2012. 216: p. 397–408.

10    Erwin L. Hahn Institute    Annual Report 2013    11

# 7th Erwin L. Hahn Lecture

The location: The red dot museum

Virtual institute meets institute

Time for discussions

The audience

The lecture: Unexpected Tomography: From Magnetic to Electrical Imaging with MRI

The 1st Erwin L. Hahn Institute Award for Young Scientists

And finally some drinks

# Current Grants

Timmann D, Cerebellar-Cortical Control: Cells, Circuits, Computation and Clinic; Marie Curie Initial Training Grant, EU; duration 4 years (January 2010 – December 2013)

Scheenen T, Exploring the aggressiveness of prostate cancer to enable an individualised treatment approach. European Research Council; duration 5 years (March 2010 – February 2015)

Timmann D, Ladd ME. Contribution of the human cerebellum to extinction learning and renewal, Project in the Research Unit FOR 1581; German Research Foundation; duration 3 years (January 2011 – December 2013)

Ladd ME, MRexcite: Unlocking the potential of ultra-high-fild MRI through manipulation of radiofrequency excitation fields in human tissue. European Research Council, duration 5 years (May 2012 – April 2017)

Norris DG, Tendolkar, Wiltfang et.al., Imaging and Curing Environmental Metabolic Diseases (ICEMED). Helmholtz-Gesellschaft; duration 5 years (July 2012 – June 2017)

Ladd ME, Norris DG, et.al., HiMR: Ultra-High Field Magnetic Resonance Imaging    Marie Curie Actions - Initial Training Networks, EU; duration 4 years (November 2012 - October 2016)

Ladd ME, Speck O, Norris DG, German Ultrahigh Field Imaging (GUFI. German Research Foundation; duration 3 years (October 2013 – September 2016)

# Personnel

New in 2013
  Lauren Bains
  Sascha Brunheim
  Martine Flöser
  Donghyun Hong
  Fabian Kahl
  Tim van Mourik
  Mark Obermann
  Seyedmorteza Rohani Rankouhi
  Anna Steinhoff
  Kira Schulz
  Michael Schwarz
  Jan-Willem Thielen
  Maximilian Völker

Left in 2013
  Andreas Botschkowski
  Simone Brunn
  Michael Kleinnijenhuis
  Kira Schulz
  Roxana Stefanescu

# Publications

Dammann, P., Wrede, K. H., Maderwald, S., Hindy, N. E., Mueller, O., Chen, B., Zhu, Y., Hütter, B., Ladd, M. E., Schlamann, M., Sandalcioglu, I., Sure, U. (2013). The venous angioarchitecture of sporadic cerebral cavernous malformations: a susceptibility weighted imaging study at 7 T MRI. Journal of neurology, neurosurgery, and psychiatry, 84(2), 194-200.

Eichner, C., Setsompop, K., Koopmans, P., Lützkendorf, R., Norris, D. G., Turner, R., Wald, L., Heidemann, R. (2013). Slice accelerated diffusion-weighted imaging at ultra-high field strength. Magnetic resonance in medicine.

Fischer, A., Kraff, O., Orzada, S., Nensa, F., Schäfer, L., Ladd, M. E., Umutlu, L., Lauenstein, T. (2013). Ultrahigh-Field Imaging of the Biliary Tract at 7 T: Initial Results of Gadoxetic Acid-Enhanced Magnetic Resonance Cholangiography. Investigative radiology.

Fischer, A., Maderwald, S., Orzada, S., Johst, S., Schäfer, L., Ladd, M. E., Nassenstein, K., Umutlu, L., Lauenstein, T. (2013). Nonenhanced Magnetic Resonance Angiography of the Lower Extremity Vessels at 7 Tesla: Initial Experience. Investigative radiology, 48(7), 525-34.

Gizewski, E., Maderwald, S., Linn, J., Dassinger, B., Bochmann, K., Forsting, M., Ladd, M. E. (2013). High-resolution anatomy of the human brain stem using 7-T MRI: improved detection of inner structures and nerves. Neuroradiology.

Grum, D., Franke, S., Kraff, O., Heider, D., Schramm, A., Hoffmann, D., Bayer, P. (2013). Design of a modular protein-based MRI contrast agent for targeted application. PloS one, 8(6), e65346.

Johst, S., Orzada, S., Fischer, A., Umutlu, L., Ladd, M. E. & Maderwald, S. (2013). Comparison of Fat Saturation Techniques for Single-Shot Fast Spin Echo Sequences for 7-T Body Imaging. Investigative radiology.

Kinner, S., Maderwald, S., Albert, J., Parohl, N., Corot, C., Robert, P., Baba, H., Barkhausen, J. (2013). Discrimination of Benign and Malignant Lymph Nodes at 7.0T Compared to 1.5T Magnetic Resonance Imaging Using Ultrasmall Particles of Iron Oxide: A Feasibility Preclinical Study. Academic radiology, 20(12), 1604-9.

Kraff, O., Wrede, K. H., Schoemberg, T., Dammann, P., Noureddine, Y., Orzada, S., Ladd, M. E., Bitz, A. K. (2013). MR safety assessment of potential RF heating from cranial fixation plates at 7 T. Medical physics, 40(4).

Küper, M., Wünnemann, M., Thürling, M., Stefanescu, R., Maderwald, S., Elles, H., Göricke, S., Ladd, M. E., Timmann, D. (2013). Activation of the cerebellar cortex and the dentate nucleus in a prism adaptation fMRI study. Human brain mapping.

Ladd, M. E. & Bock, M. (2013). [Problems and chances of high field magnetic resonance imaging.]. Der Radiologe, 53(5), 401-10.

Lagemaat, M., Vos, E., Maas, M., Bitz, A. K., Orzada, S., van Uden, M., Kobus, T., Heerschap, A., Scheenen, T. (2013). Phosphorus Magnetic Resonance Spectroscopic Imaging at 7 T in Patients With Prostate Cancer. Investigative radiology.

Maas, M., Vos, E., Lagemaat, M., Bitz, A. K., Orzada, S., Kobus, T., Kraff, O., Maderwald, S., Ladd, M. E., Scheenen, T. (2013). Feasibility of T2 -weighted turbo spin echo imaging of the human prostate at 7 tesla. Magnetic resonance in medicine.

Norris, D. G., Boyacioǧlu, R., Schulz, J., Barth, M. & Koopmans, P. (2013). Application of PINS radiofrequency pulses to reduce power deposition in RARE/turbo spin echo imaging of the human head. Magnetic resonance in medicine.

Poser, B., Barth, M., Goa, P., Deng, W. & Stenger, V. (2013). Single-shot echo-planar imaging with Nyquist ghost compensation: Interleaved dual echo with acceleration (IDEA) echo-planar imaging (EPI). Magnetic resonance in medicine, 69(1), 37-47.

Risius, U., Staniloiu, A., Piefke, M., Maderwald, S., Schulte, F., Brand, M., Markowitsch, H. (2013). Retrieval, monitoring, and control processes: a 7 tesla FMRI approach to memory accuracy. Frontiers in behavioral neuroscience, 7, 24.

Stefanescu, M., Thürling, M., Maderwald, S., Wiestler, T., Ladd, M. E., Diedrichsen, J., Timmann, D. (2013). A 7T fMRI study of cerebellar activation in sequential finger movement tasks. Experimental brain research. Experimentelle Hirnforschung. Experimentation cerebrale, 228(2), 243-54.

Theysohn, J., Kraff, O., Maderwald, S., Kokulinsky, P., Ladd, M. E., Barkhausen, J., Ladd, S. C. (2013). MRI of the ankle joint in healthy non-athletes and in marathon runners: image quality issues at 7.0 T compared to 1.5 T. Skeletal radiology, 42(2), 261-7.

Theysohn, J., Kraff, O., Orzada, S., Theysohn, N., Classen, T., Landgraeber, S., Ladd, M. E., Lauenstein, T. (2013). Bilateral hip imaging at 7 Tesla using a multi-channel transmit technology: initial results presenting anatomical detail in healthy volunteers and pathological changes in patients with avascular necrosis of the femoral head. Skeletal radiology, 42(11), 1555-63.

Theysohn, N., Qin, S., Maderwald, S., Poser, B., Theysohn, J., Ladd, M. E., Norris, D. G., Gizewski, E., Fernandez, G., Tendolkar, I. (2013). Memory-Related Hippocampal Activity Can Be Measured Robustly Using fMRI at 7 Tesla. Journal of neuroimaging: official journal of the American Society of Neuroimaging, 23(4), 445-451.

Umutlu, L., Bitz, A. K., Maderwald, S., Orzada, S., Kinner, S., Kraff, O., Brote, I., Ladd, S. C., Schroeder, T., Forsting, M., Antoch, G., Ladd, M. E., Quick, H., Lauenstein, T. (2013). Contrast-enhanced ultra-high-field liver MRI: A feasibility trial. European journal of radiology, 5(82), 760-5.

Umutlu, L., Kraff, O., Fischer, A., Kinner, S., Maderwald, S., Nassenstein, K., Nensa, F., Grüneisen, J., Orzada, S., Bitz, A. K., Forsting, M., Ladd, M. E., Lauenstein, T. (2013). Seven-Tesla MRI of the female pelvis. European radiology, 23(9), 2364-73.

Umutlu, L., Ladd, M. E., Forsting, M. & Lauenstein, T. (2013). 7 Tesla MR Imaging: Opportunities and Challenges. RoFo: Fortschritte auf dem Gebiete der Rontgenstrahlen und der Nuklearmedizin.

Umutlu, L., Maderwald, S., Kinner, S., Kraff, O., Bitz, A. K., Orzada, S., Johst, S., Wrede, K. H., Forsting, M., Ladd, M. E., Lauenstein, T., Quick, H. (2013). First-pass contrast-enhanced renal MRA at 7 Tesla: initial results. European radiology, 23(4), 1059-66.

Umutlu, L., Theysohn, N., Maderwald, S., Johst, S., Lauenstein, T., Moenninghoff, C., Goericke, S., Dammann, P., Wrede, K., Ladd, M. E., Forsting, M., Schlamann, M. (2013). 7 Tesla MPRAGE Imaging of the Intracranial Arterial Vasculature: Nonenhanced versus Contrast-Enhanced. Academic radiology, 20(5), 628-34.

Zahedi, Y., Zaun, G., Maderwald, S., Orzada, S., Pütter, C., Scherag, A., Winterhager, E., Ladd, M. E., Grümmer, R. (2013). Impact of repetitive exposure to strong static magnetic fields on pregnancy and embryonic development of mice. Journal of magnetic resonance imaging.

Zaun, G., Zahedi, Y., Maderwald, S., Orzada, S., Pütter, C., Scherag, A., Winterhager, E., Ladd, M. E., Grümmer, R. (2013). Repetitive exposure of mice to strong static magnetic fields in utero does not impair fertility in adulthood but may affect placental weight of offspring. Journal of magnetic resonance imaging.

## Erwin L. Hahn Institute for Magnetic Resonance Imaging

Arendahls Wiese 199
D-45141 Essen
Germany

t ++49 (0)201-183-6070
f ++49 (0)201-183-6073
w www.hahn-institute.de